Organic Electronics 13 (2012) 2910–2916

Contents lists available at SciVerse ScienceDirect

Organic Electronics

journal homepage: www.elsevier.com/locate/orgel

Reliable extraction of organic solar cell parameters by combining steady-state and transient techniques

M.T. Neukom [a,b,*], S. Züfle [a], B. Ruhstaller [a,b]

[a] Institute of Computational Physics, ZHAW, Zurich University of Applied Sciences, Technikumstr. 9, 8401 Winterthur, Switzerland
[b] Fluxim AG, Dorfstrasse 7, 8835 Feusisberg, Switzerland

ARTICLE INFO

Article history:
Received 20 July 2012
Received in revised form 30 August 2012
Accepted 2 September 2012
Available online 28 September 2012

Keywords:
Numerical simulation
Parameter extraction
CELIV
Characterization
Charge carrier mobility
Parameter correlation

ABSTRACT

A method to extract reliable material and device parameters of organic solar cells is presented. We employ a comprehensive numerical device model to simulate the solar cell operation in transient and steady-state condition. Parameter extraction with numerical simulation is error-prone because model parameters are often correlated, their unique determination is very difficult and extracted parameters are likely to be inaccurate. We combine the current–voltage characteristics, the photo-CELIV currents (charge extraction with linearly increasing voltage) and the photocurrent response to a light pulse to reduce parameter correlation and increase accuracy and reliability of the extracted parameters. With a correlation matrix analysis it is shown that parameter correlation is significantly reduced when combining several experimental data sets compared with the analysis of current–voltage curves only. We find a set of parameters to reproduce the complete series of measurements with the numerical simulation. The full electrical behavior can be described using a basic drift–diffusion model with constant mobilities and direct photon-to-charge conversion. With this model we extract charge carrier mobilities in the order of 10^{-4} cm^2/V s, a Langevin recombination prefactor of 0.08, charge injection barriers equal at both sides in the range of 0.25 eV and further device parameters for a BHJ cell with PT5DPP as donor and PCBM (C70) as acceptor. The solar cell is simulated with the extracted parameters and internal distribution of electrons, holes and the electric field are visualized.

1. Introduction

Improving the efficiency of organic solar cells requires the understanding of the physical processes and determination of material parameters for light absorption and charge transport. In order to extract material and device parameters from the experimental data either simple analytical or complex numerical approaches are used.

Analytical models are based on simplified assumptions and do not consider all physical effects that are relevant. The extracted parameters therefore often lack accuracy [1]. These techniques may only be used to determine the order of magnitude of a parameter or to compare one device with another.

To account for more physical effects numerical simulation is required since analytical solutions do not exist in general. Because the models are usually complex the number of unknown parameters can be large. With a large number of unknown parameters accurate parameter extraction gets very difficult because parameters are often correlated and have a similar influence on the result.

There have been many efforts in the past to develop and employ numerical device models to describe charge transport in organic solar cells. Barker et al. [2] simulated current–voltage characteristics of a bilayer organic solar cells with a drift–diffusion model, Koster et al. [3] developed a model to simulate bulk-heterojunction solar cells. Häusermann and co-workers [4] studied the influence of parameters for charge-transfer excitons by simulation of current–voltage characteristics and light pulse transients. Hwang et al. [5,6] used a time-dependent drift–diffusion

* Corresponding author. Tel.: +41 (0)58 934 74 88.
E-mail address: martin.neukom@fluxim.com (M.T. Neukom).

1566-1199/$ - see front matter © 2012 Elsevier B.V. All rights reserved.
http://dx.doi.org/10.1016/j.orgel.2012.09.008

model to fit photo-current transients at different negative voltages. Christ and co-workers [7] studied the photo-current response to a short laser flash with numerical simulation of the optical and electrical processes including charge traps. In a previous study [8,1] we simulated the CELIV experiment with a numerical drift–diffusion model to extract material and device parameters.

Some of the mentioned authors determined material parameters with additional experiments like time-of-flight for charge carrier mobilities or cyclo-voltammetry for the HOMO and LUMO levels. When a device is built the individual material parameters change slightly and need to be adapted. The individually determined material parameters can therefore be used as an adequate starting point for the optimization as shown in Section 3.3.

In all these studies only one single measurement technique is investigated at once. In this study we combine several techniques and show that the parameter correlation can be reduced significantly compared to the case when only analyzing current–voltage characteristics. We calculate the correlation matrix for the combination of all experiments to quantify the significantly reduced parameter correlation.

With one model and one set of parameters the current–voltage characteristics, the photocurrent response to a light pulse, the dark-CELIV currents and the photo-CELIV current are reproduced. Because these techniques are complementary the model parameters have a different influence on the various experiments. This reduction in correlation leads to more accurate and more reliable parameters.

2. Experimental

In this study a device with a novel small bandgap *p*-type polymer PT5DPP (Fig. 1) provided by BASF blended with PCBM (C70) is investigated. The device is provided by CSEM and fabricated by spin-coating PEDOT:PSS and the active polymer blend onto a glass substrate with pre-structured ITO electrodes. The layer structure is ITO (75 nm), PEDOS:PSS (60 nm), PT5DPP:PCBM (C70)(1:2) (90 nm), LiF (1 nm), and Aluminium (100 nm). The active area of the solar cell is 0.04 cm^2.

We illuminate the solar cell with a blue LED with a peak wavelength of 468 nm. The LED is driven by an arbitrary waveform generator. The maximum light intensity of the LED (γ = 1.0) is 281 W/m^2. A second arbitrary waveform generator is used to apply the cell voltage. The current is measured over a shunt resistance with a digital storage oscilloscope.

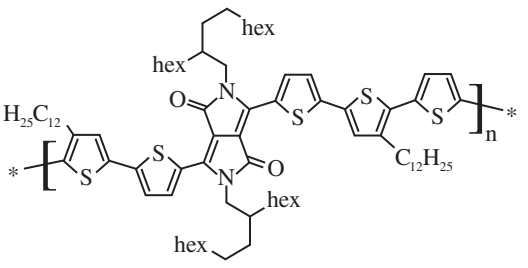

Fig. 1. Chemical structure of PT5DPP (BASF).

The same measurement setup is used for all techniques and all the measurements are performed automated and within minutes after each other. By measuring everything in a very short period of time we ensure that the cell does not change and temperature as well as other environmental conditions are constant. Using the same measurement setup for all measurements all systematic errors of the measurement devices as well as contact resistance remain the same. The measured curves are therefore very consistent.

3. Model

3.1. Physical model

In this study we use a fully-coupled opto-electrical model to analyze the experimental curves. The model is implemented in the *semiconducting emissive thin film optical simulator* (SETFOS) [1,4,8,9].

The spectrum of the blue LED is used to calculate the optical light penetration and the photon absorption profile inside the active layer. To scale the illumination spectrum according to the measurements the factor γ is used where γ = 1.0 is the maximum light intensity.

In the electrical model the photon absorption profile is used to directly generate free electrons and holes. Conversion losses are considered with the photon-to-charge conversion efficiency η_{p2c}. The one dimensional drift–diffusion calculation is performed for electrons and holes with Langevin recombination and thermionic injection. The series-resistance of the electric circuit is considered in the electrical simulation as illustrated in Fig. 2. Taking the series-resistance into account is important since it has a significant influence on the transient and steady-state simulation results [1]. The effective applied voltage V_{App} at the device is calculated as

$$V_{App} = V_{Source} - j_{tot} \cdot S \cdot R_s \quad (1)$$

where V_{Source} is the ideal voltage source, j_{tot} is the total current density through the device and S is the device surface. The series resistance R_S represents all resistances in the measurement circuit like shunt, contact or ITO resistance.

In this paper the notation of built-in voltage and injection barriers is used as

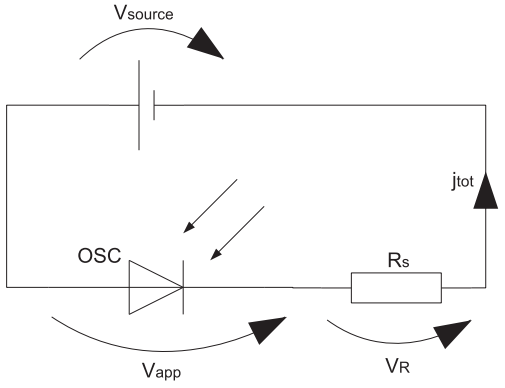

Fig. 2. Sketch of the electrical circuit used in the simulation model.

$$V_{bi} = \frac{\Phi_{anode} - \Phi_{cathode}}{q} \quad (2)$$

$$\Delta_{anode} = \mathrm{HOMO} - \Phi_{anode} \quad (3)$$

$$\Delta_{cathode} = \Phi_{cathode} - \mathrm{LUMO} \quad (4)$$

where V_{bi} is the built-in voltage, Φ_{anode} and $\Phi_{cathode}$ are the work functions of the electrodes, q is the unit charge, Δ_{anode} and $\Delta_{cathode}$ are the injection energy barriers, HOMO is the highest occupied molecular orbital energy and LUMO is the energy of the lowest unoccupied molecular orbit.

Advanced models and effects like CT-excitons, doping, traps or extended Gaussian disorder model EGDM are not considered in this study since already the simplified model leads to good fits. A detailed description of the optical and electrical simulation can be found in one of our previous publications [1].

3.2. Method to analyze parameter correlation

To quantify the linear correlation between two parameters the correlation coefficient is calculated for all parameter combinations and illustrated in the correlation matrix. The correlation coefficient indicates whether varying one parameter has the same influence on all the errors (deviation between measurement and simulation) as varying the other parameter.

For this analysis the Jacobian matrix

$$J_{ij} = \frac{df_i}{dp_j} \quad (5)$$

is calculated where f_i are the errors (deviation between measurement and simulation) and p_j are the model parameters. The use of appropriate error functions f is crucial for good results as we show in Section 3.3. With the Jacobian matrix J the covariance matrix C is calculated as

$$C = (J^T \cdot J) \quad (6)$$

To obtain the correlation matrix M the covariance matrix is normalized according to

$$M_{ij} = \frac{C_{ij}}{\sqrt{C_{ii} \cdot C_{jj}}}. \quad (7)$$

The correlation matrix M contains values between -1 and 1. A value close to zero indicates no linear correlation between the parameter in the column and the parameter of the row. A value of -1 or 1 indicates full negative or positive correlation. The diagonal of a correlation matrix is always 1 as a parameter is always positively correlated with itself.

In non-linear optimization the covariance matrix C is often inverted. It can lead to confusion that this inverted matrix is sometimes also called the covariance matrix. The elements of the inverted matrix can be interpreted as partial correlation or partial variances between parameters. The correlation matrix and covariance matrix analyzed in this study shall not be confused with the inverted covariance matrix.

3.3. Method for parameter extraction

In this section a method to extract parameters of organic solar cells is described. The model for the simulations in this study has three important device parameters: the built-in voltage V_{bi}, the anode injection barrier Δ_{anode} and the cathode injection barrier $\Delta_{cathode}$. There are additional six parameters to describe charge transport in the material: electron mobility μ_n, hole mobility μ_p, bimolecular recombination efficiency η_R, photon-to-charge conversion efficiency η_{p2c}, the density of chargeable sites N_0 and the relative permittivity ϵ_r. Together with the series resistance R_S there are ten unknown parameters.

The first parameter to be evaluated independently is the series resistance R_S of the measurement setup. A small voltage step at negative bias is applied to the device (in our example a step from -0.5 V to -0.6 V seemed to be favorable). In this voltage range charge injection can be neglected and only the displacement current is measured. The series resistance R_S is given by

$$R_S = \frac{\Delta V}{I_0} \quad (8)$$

where ΔV is the voltage step and I_0 the height of the current peak. As an alternative the series resistance can also be evaluated from the initial current slope of the dark CELIV experiment as described in reference [1].

The relative permittivity ϵ_r is evaluated analyzing the displacement current in the dark CELIV experiment. In the CELIV technique a linearly increasing voltage $V(t) = A \cdot t$ is applied to the device. After extraction of the intrinsic charge carriers only the displacement current j_0 is measured. The relative permittivity is then evaluated according to

$$\epsilon_r = \frac{j_0 \cdot d}{A \cdot \epsilon_0} \quad (9)$$

where d is the thickness of the active layer, A is the voltage slope and ϵ_0 is the vacuum permittivity.

To obtain the photon-to-charge conversion efficiency η_{p2c} the steady-state photocurrent is analyzed for different light intensities at negative bias voltage. The negative voltage leads to a high electric field inside the bulk and an efficient extraction of electrons and holes. In this state, recombination can be neglected and all charge carriers are extracted. The current therefore only depends on the photon-to-charge efficiency and the light intensity. If the absolute illumination intensity is known the photon-to-charge conversion efficiency η_{p2c} can be identified as the slope of the photocurrent versus illumination intensity.

There are seven parameters left that cannot be determined individually. A fitting algorithm is used to obtain these parameters. To achieve convergence of the algorithm it is important to start with a good initial guess for the set of parameters.

The order of magnitude of the electron mobility[1] μ_n can be determined with CELIV using the Juska-formula [10] or one of its derivations [11–13].

[1] With CELIV usually only the mobility of the faster charge carrier can be determined. We assume the electrons to be faster in the materials used in this study.

The initial guess for the built-in voltage, the anode barrier and the cathode barrier are chosen according to the energy diagram with the HOMO and LUMO level of the active layer and the work-functions of the electrodes.

The density of chargeable sites N_0 is estimated as

$$N_0 = \frac{1}{a^3} \tag{10}$$

where a is the average molecular distance.

Fitting seven parameters simultaneously requires much information from measurements to be able to find a unique solution. Therefore three complementary measurement techniques are used:

1. *Current–voltage characteristics*. The current–voltage characteristics in the dark and illuminated with varied light intensities is analyzed.
2. *Transient photocurrent response to a light pulse*. The cell is illuminated for 20μs and the short-circuit current is analyzed for varied illumination intensities.
3. *CELIV and photo-CELIV*. The CELIV experiment as described by Juska et al. [10] is performed in the dark (dark-CELIV) and with a light pulse (photo-CELIV). In both cases the voltage slope A is varied. In the photo-CELIV experiment the cell is illuminated with light intensity $\gamma = 1.0$ and biased ($V_{App} = 0.57$ V) to prevent a current flow prior to the voltage pulse. The illumination is turned off 3μs before the voltage ramp starts.

The Levenberg–Marquardt [14,15] nonlinear least square algorithm is applied to fit the simulations to all measurement curves simultaneously. All parameters are mapped linearly or logarithmically onto a scale from 0 to 1 ensuring that the order of magnitude has no influence on the optimization. The Levenberg–Marquardt algorithm requires the Jacobian matrix J as an input and determines a parameter-set h for the next iteration according to

$$(J^T \cdot J + \mu \cdot I) \cdot h = -J^T \cdot f \tag{11}$$

where μ is the damping parameter, I is the identity matrix and f are the actual fitting errors.

Choosing appropriate error definitions f to calculate the Jacobian matrix for the different measurement curves is key to good convergence of the algorithm. In classical optimization the errors are defined through different points on the measured and simulated curves. To improve convergence we implement a custom error definition. Thus the influence of the various parameters on the errors f can be separated to some extent. This leads to a Jacobian matrix that is favorable for the convergence of the optimizer.

For the current–voltage curves the following errors were defined: the difference in open-circuit voltage, short-circuit current, the slope of the injection current at 0.7 V, the normalized shape of the curve in the fourth quadrant and the integral of the deviation between measurement and simulation.

For the transient photo-current response the integral of the deviation of measurement and simulation and the integral of the normalized difference were used as error functions.

For the CELIV measurements the peak-height, the peak-time and the integral of the curve-deviation were defined as errors.

The errors are weighted with individual factors (values between 0.1 and 10) in order to further reduce the parameter correlation. Error definitions that have a more orthogonal influence are weighted higher so the sum of all correlations is minimized.

4. Results and discussion

The JV-curve, the transient current response to a light pulse, dark-CELIV and photo-CELIV currents have been measured on an organic bulk heterojunction solar cell. The measurement curves are reproduced by the numerical simulation as shown in Fig. 3. The parameters used for the simulation are listed in Table 1 and were found according to the procedure described in Section 3.3. The numerical model describes all the measured curves well using just one single set of parameters.

The simulation describes the charge injection and all the steady-state physics visible in the current–voltage characteristics shown in Fig. 3a and can reproduce the measurements well for all light intensities γ.

The temporal dynamics of the generated charges moving to the electrodes can be studied with the transient photo-current response shown in Fig. 3b. The simulation can reproduce rise and decline of the current precisely for several curves with varied light intensity γ.

Fig. 3c depicts the dark-CELIV experiment with several voltage slopes A. There is no current overshoot indicating that there are no intrinsic charge carriers in the bulk in the dark. These dark-CELIV curves are mainly determined by RC-effects and can therefore be used to evaluate the resistance R_S and the electrical permittivity ϵ_r. For the case of $A = 0.5$ V/μs we observe a rise of the current due to charge injection. As charge injection in reverse bias is not considered in the device model this effect cannot be described by the simulation.

In Fig. 3d the photo-CELIV experiment is shown. After the illumination has been turned off (at $t = -3$ μs) the current density increases slightly to 2 mA/cm^2 due to charge injection. The voltage ramp starting at $t = 0$ μs leads to a displacement current and extracts the free charge carriers from the device. All these effects are well described by the simulation model.

4.1. Correlation analysis

To prove the significantly reduced parameter correlation of the simulations shown in Fig. 3 it is compared with the simulation of a JV-curve under illumination and in the dark performed with the same parameters. The Jacobian matrix J is calculated using 25 points equally distributed on the JV-curve under illumination and on the JV-curve in the dark. The correlation matrix M_{JV} is calculated and shown in Table 2. Apart from a few exceptions all the parameters are highly correlated with each other. Only three values are below 0.5. The average correlation between the parameters is 0.69. Varying one parameter can

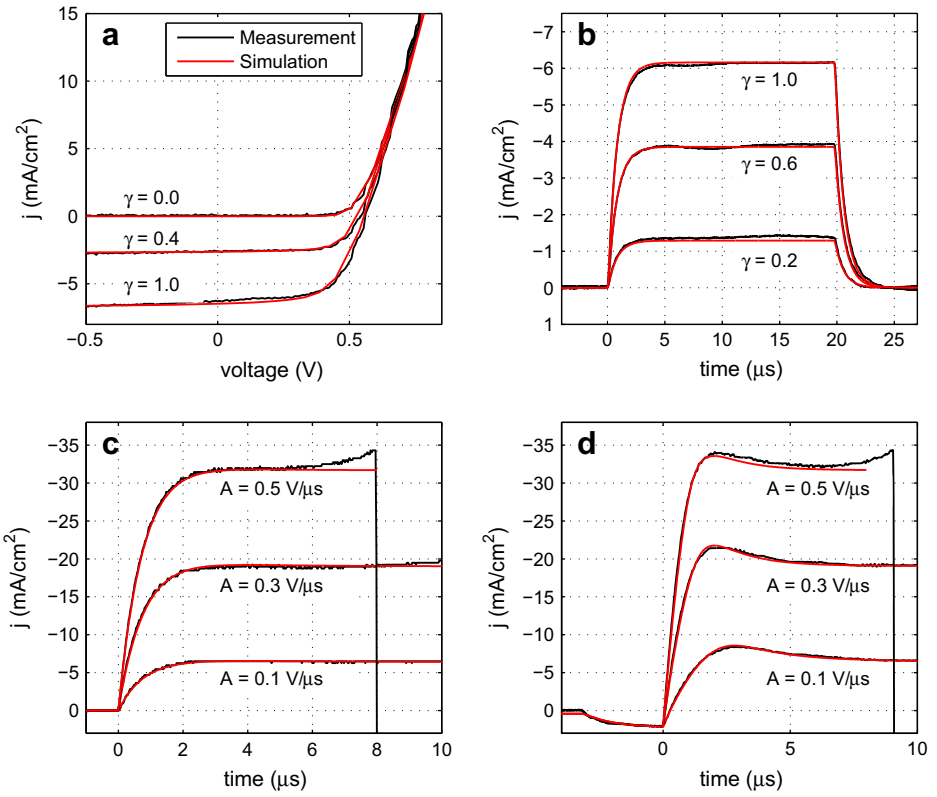

Fig. 3. (a) Simulated and measured current–voltage characteristics with varied light intensity γ. (b) Simulated and measured transient photocurrent at 0 V with varied light intensity γ. (c) Simulated and measured dark-CELIV currents with varied voltage slope A. (d) Simulated and measured photo-CELIV currents with varied voltage slope A.

therefore have a very similar influence on the simulation results as varying another parameter. Reliable determination of model parameters is therefore not possible using only two JV-curves.

Using the error definition as described in Section 3.3 the Jacobian matrix is calculated for JV-curve, current response to a light pulse and photo-CELIV. With the approach of the combined measurements parameter correlation is significantly reduced as shown in the correlation matrix M_{all} in

Table 1
Parameters used for the numerical simulation in Fig. 3.

Parameter	Symbol	Value	Unit
Material			
Electron mobility	μ_n	7.5×10^{-4}	$cm^2/V\,s$
Hole mobility	μ_p	3.5×10^{-4}	$cm^2/V\,s$
Relative permittivity	ϵ_r	6.51	1
Langevin recombination efficiency	η_R	0.08	1
Photon-to-charge conversion efficiency	η_{p2c}	0.78	1
Density of chargeable sites	N_0	3.7×10^{27}	$1/m^3$
Device			
Injection barrier anode	Δ_{anode}	0.225	eV
Injection barrier cathode	$\Delta_{cathode}$	0.235	eV
Built-in voltage	V_{bi}	0.80	V
Measurement set-up			
Series resistance	R_S	286	Ω
Illumination intensity	I_0	281	W/m^2

Table 2
Correlation matrix M_{JV} of two current–voltage curves-one under illumination, one in the dark.

	μ_n	μ_p	η_R	V_{bi}	Δ_{anode}	$\Delta_{cathode}$	N_0
μ_n	1	–	–	–	–	–	–
μ_p	0.97	1	–	–	–	–	–
η_R	0.60	0.40	1	–	–	–	–
V_{bi}	−0.51	−0.36	−0.70	1	–	–	–
Δ_{anode}	−0.83	−0.71	−0.75	0.74	1	–	–
$\Delta_{cathode}$	−0.84	−0.71	−0.80	0.89	0.91	1	–
N_0	0.74	0.65	−0.72	−0.28	−0.80	−0.60	1

Table 3
Correlation matrix M_{all} of the full measurement series with JV-curve, current response to light pulse and photo-CELIV.

	μ_n	μ_p	η_R	V_{bi}	Δ_{anode}	$\Delta_{cathode}$	N_0
μ_n	1	–	–	–	–	–	–
μ_p	0.23	1	–	–	–	–	–
η_R	0.53	0.16	1	–	–	–	–
V_{bi}	0.33	0.30	−0.29	1	–	–	–
Δ_{anode}	0.28	0.30	0.11	0.24	1	–	–
$\Delta_{cathode}$	0.30	0.35	−0.27	0.67	0.82	1	–
N_0	0.38	0.04	0.45	0.12	−0.42	−0.42	1

Table 3. The average correlation between the parameters is 0.35. Because the different measurement techniques are complementary the parameters have a different influence on the various errors. This effect is reducing the correlation.

The anode and cathode barrier correlate, as well as the cathode barrier and the built-in voltage. The extracted model parameters for built-in V_{bi}, and injection barriers Δ_{anode}, $\Delta_{cathode}$ are therefore in this case less reliable than the other parameters. All the other parameters show a very small correlation.

It needs to be mentioned that this correlation analysis only considers linear correlation. Quadratic or any other type of correlation is still possible even if the correlation coefficient is low. The correlation matrix should therefore not be over-interpreted but is an appropriate method to monitor correlation and is a good indication for accurate and reliable parameter extraction.

4.2. Internal charge and electric field distribution

In the previous section the accuracy and reliability of the model parameters have been discussed. These parameters are now used to investigate the charge and electric field distribution inside the bulk for different operating conditions. As these quantities are not accessible via measurement only numerical simulation allows to get an insight into the device.

In Fig. 4 the distribution of electrons and holes inside the device is illustrated whereas $x = 0$ is the anode interface and $x = d = 90$ nm is the cathode interface. Fig. 5 shows the electric field accordingly.

At short-circuit conditions ($V = 0$) the concentration of electrons and holes in the middle of the device is low because the electric field is high and charge carriers are transported to the electrodes by drift. The holes are concentrated near the anode and exponentially declining, the electrons are near the cathode, respectively. This is a result of charges being injected and diffusing inside the bulk whereas the drift current flows in the opposite direction. At open circuit conditions ($V = V_{oc}$) the electric field inside the bulk is low such that drift and diffusion currents compensate each other. The amount of charge carriers inside the cell is therefore much higher (in this case a factor of 20) compared with the short circuit case. All the generated charge carriers then annihilate by bimolecular recombination. In maximum power point condition ($V = V_{MPP}$) the charge carriers and electric field distribution is between the extrema of short-circuit and open-circuit.

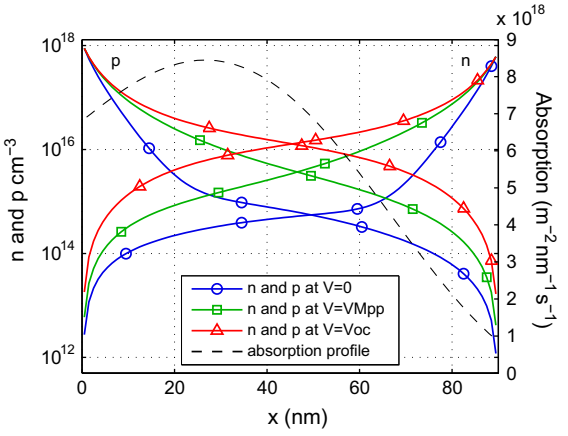

Fig. 4. Internal distribution of electrons and holes calculated using parameters in Table 1 at operating point $V = 0$, $V = V_{MPP}$, $V = V_{oc}$. The dashed line illustrates the absorption profile.

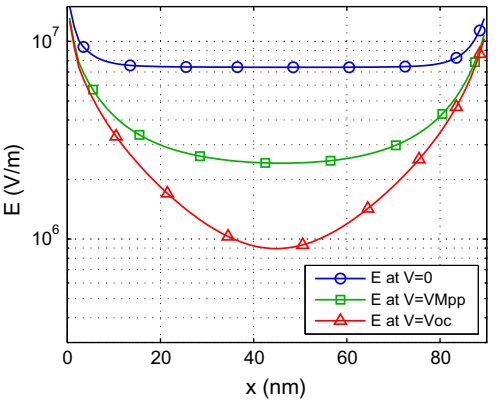

Fig. 5. Internal distribution of the electric field calculated using parameters in Table 1 at operating point $V = 0$, $V = V_{MPP}$, $V = V_{oc}$.

In Fig. 4 also the absorption profile is illustrated with the dashed line. In this solar cell both mobilities are high enough that charge extraction rather than charge transport is the limiting factor. Therefore the position of the absorption peak is not of major importance for the cell efficiency.

5. Conclusions

We describe the electrical transport of an organic bulk-heterojunction solar cell for various experiments with one model and one single set of parameters. The steady-state effects of the current–voltage characteristics as well as the time dynamics of the transient photo-current response and the CELIV experiment can be reproduced accurately with a simple drift–diffusion model with constant mobilities. More detailed effects and models like charge trapping, mobilities depending on the electric field or CT-excitons are not required to describe the solar cell used in this study. In order to keep the amount of unknown parameters low it is recommended to use the most simple model for the extraction of parameters and only to resort to more comprehensive models if this approach fails. Advanced models can be used if additional parameters can be accessed with other complementary experiments.

We presented a technique to derive all parameters of this model and show that parameter correlation is significantly reduced by calculating a correlation matrix.

The presented method for parameter extraction can be used for further studies like monitoring trends of aging or investigating the influence of layer thickness, morphology or material variations. To further improve the method and increase the reliability of the extracted parameters additional experiments as impedance spectroscopy or

injection-CELIV as recently presented by Juska et al. [16] can be included in the portfolio of experiments.

Acknowledgments

The organic semiconductors, cyclo-voltammetry and ellipsometry measurements were kindly provided by Mathieu Turbiez and colleagues at BASF in Basel. We thank Ton Offermans and colleagues at CSEM Muttenz for the fabrication of the organic solar cells. The authors gratefully acknowledge financial support from the Swiss Federal Office of Energy and the European Commission for supporting the project *Apollo* and *Sunflower* [17] respectively.

References

[1] M.T. Neukom, N.A. Reinke, B. Ruhstaller, Sol. Energy 85 (2011) 1250.
[2] J.A. Barker, C.M. Ramsdale, N.C. Greenham, Phys. Rev. B 67 (2003) 075205.
[3] L.J.A. Koster, E.C.P. Smits, V.D. Mihailetchi, P.W.M. Blom, Phys. Rev. B 72 (2005) 085205.
[4] R. Häusermann, E. Knapp, M. Moos, N.A. Reinke, T. Flatz, B. Ruhstaller, J. Appl. Phys. 106 (2009) 104507.
[5] I. Hwang, N.C. Greenham, Nanotechnology 19 (2008) 424012.
[6] I. Hwang, C.R. McNeill, N.C. Greenham, J. Appl. Phys. 106 (2009) 094506.
[7] N.S. Christ, S.W. Kettlitz, S. Valouch, S. Züfle, C. Gärtner, M. Punke, U. Lemmer, J. Appl. Phys. 105 (2009) 104513.
[8] M.T. Neukom, N.A. Reinke, K.A. Brossi, B. Ruhstaller, Proc. SPIE 7722 (2010) 77220V.
[9] Semiconducting thin film optics simulator (SETFOS) by Fluxim AG, Switzerland, <www.fluxim.com>.
[10] G. Juska, K. Arlauskas, M. Viliunas, J. Kocka, Phys. Rev. Lett. 84 (2000) 4946.
[11] G. Juska, M. Viliunas, K. Arlauskas, N. Nekrases, N. Wyrsch, L. Feitknecht, J. Appl. Phys. 89 (2001) 4971.
[12] S. Bange, M. Schubert, D. Neher, Phys. Rev. B 81 (2010) 035209.
[13] J. Lorrmann, B.H. Badada, O. Inganäs, V. Dyakonov, C. Deibel, J. Appl. Phys. 108 (2010) 113705.
[14] K. Levenberg, Quart. Appl. Math. 2 (1944) 164.
[15] JD. Marquardt, SIAM J. Appl. Math. 11 (1963) 431.
[16] G. Juska, N. Nekrasas, K. Genevicius, J. Non-Cryst. Solids 358 (2012).
[17] FP7 Project Sunflower, <www.sunflower-fp7.eu>.